Planetary Probe Entry Atmosphere Estimation Using Synthetic Air Data System

Christopher D. Karlgaard*

Analytical Mechanics Associates, Inc., Hampton, VA

Mark Schoenenberger†

NASA Langley Research Center, Hampton, VA

This paper develops an atmospheric state estimator based on inertial acceleration and angular rate measurements combined with a vehicle aerodynamic model. The approach utilizes the navigation state of the vehicle to recast the vehicle aerodynamic model to be a function solely of the atmospheric state. Force and moment measurements are based on vehicle sensed accelerations and angular rates. These measurements are combined with an aerodynamic model and a Kalman-Schmidt filter to estimate the atmospheric conditions. The method is applied to data from the Mars Science Laboratory mission, which landed the Curiosity rover on the surface of Mars in August 2012. The results of the estimation algorithm are compared with results from a Flush Air Data Sensing algorithm based on onboard pressure measurements on the vehicle forebody. The comparison indicates that the proposed method provides estimates consistent with the air data measurements, without the use of pressure transducers. Implications for future missions such as the Mars 2020 entry capsule are described.

Nomenclature

C	=	state-parameter covariance
$\mathcal{F}$	=	aerodynamic force, N
F	=	linearization of $\boldsymbol{f}$ with respect to $\boldsymbol{x}$
$\boldsymbol{f}$	=	process model
G	=	linearization of $\boldsymbol{f}$ with respect to $\boldsymbol{u}$
g	=	gravitational acceleration, m/s^2
H	=	linearization of $\boldsymbol{h}$ with respect to $\boldsymbol{x}$
$\boldsymbol{h}$	=	measurement model
I	=	identity matrix

---

*Supervising Engineer, Senior Member AIAA.

†Aerospace Engineer, Atmospheric Flight and Entry Systems Branch, Senior Member AIAA.

American Institute of Aeronautics and Astronautics

$\mathcal{I}$	=	vehicle inertia, kg-m^2
i	=	iteration counter
$\boldsymbol{K}$	=	filter gain
k	=	integer time index
$\boldsymbol{L}$	=	linearization of $\boldsymbol{h}$ with respect to $\boldsymbol{u}$
$\mathcal{M}$	=	aerodynamic moment, N-m
M	=	Mach number
$\boldsymbol{P}$	=	covariance of $\boldsymbol{x}$
p_s	=	static pressure, Pa
$\boldsymbol{Q}$	=	process noise spectral density
$\tilde{\boldsymbol{Q}}$	=	process noise covariance
$\boldsymbol{R}$	=	measurement error covariance matrix
$\Re$	=	specific gas constant, J/kg-K
r	=	radius, m
T	=	atmospheric temperature, K
$\boldsymbol{u}$	=	aerodynamic model parameters
v_n, v_e, v_d	=	vehicle planet-relative north, east, and down velocity components, m/s
w_n, w_e, w_d	=	north, east, and down wind velocity components, m/s
$\boldsymbol{x}$	=	atmospheric state vector
Θ	=	longitude, rad
θ, ϕ, ψ	=	vehicle pitch, roll, and yaw attitude angles, rad
Λ	=	declination, rad
$\boldsymbol{\lambda}$	=	aerodynamic database uncertainty factors
μ	=	gravitational parameter, m^3/s^2
$\boldsymbol{\nu}$	=	vehicle inertial state
ρ	=	density, kg/m^3
$\boldsymbol{\Phi}$	=	state transition matrix

I.   Introduction

NASA has developed an Entry, Descent, and Landing (EDL) technology development roadmap [1] to guide investment strategies for increased EDL capabilities and robustness. One area of emphasis is on the development of precision landing capabilities achieved through improved environment/atmosphere characterization and EDL instrumentation for validation of engineering models and ground testing procedures. One approach that can be used to address these areas is the implementation of a Flush Air Data Sensing (FADS) system, which utilizes an array of pressure ports installed in the vehicle forebody to measure the pressure distribution during entry. These pressure measurements can be processed to estimate the freestream aerodynamic state (such as flow angles, Mach number, and dynamic pressure), atmospheric conditions (density, pressure, and winds), and vehicle aerodynamics. These sensors can be used for post-flight trajectory reconstruction and model validation, but also have the potential to be used to augment the on-board flight control system by providing estimates of density and wind velocity if the data processing algorithms can be implemented in real-time, assuming that suitable guidance and control algorithms

American Institute of Aeronautics and Astronautics

exist that can use this information. In one recent example [2], the direct force control method to entry guidance has been shown to greatly reduce fuel usage for human class Mars missions. The direct force control method differs from previously utilized bank angle modulation methods in that lift and side forces are controlled directly in the guidance algorithm. The direct force control method thus utilizes the freestream flow angles (angles of attack and sideslip) in the feedback loop for controlling lift and side force. It is expected that a sensor system that can provide real-time data can further enhance the on-board guidance performance by providing estimates of the true aerodynamic flow angles rather than inertial estimates of the angles.

Incorporation of pressure transducers into the heatshield of an entry vehicle is not trivial. Implementation of a reliable FADS system typically involves hardware development and qualification, optimization of pressure port layout, sensor calibration, ground testing to ensure pressure port and thermal protection system integrity, etc., which can be costly. Additionally, a FADS system is subject to risks of sensor failures and other hardware anomalies. Thus, backup systems are required for robustness in the event of a FADS sensor failure. One approach is to utilize a vehicle aerodynamic model in place of the sensor measurements to provide estimates of the freestream conditions.

The concept of utilizing vehicle aerodynamic models for entry probe atmosphere estimation is not new. In fact, the concept goes back to a 1963 NASA report [3] in which a proposal was made to "invert" the entry physics problem by solving for atmospheric density, given acceleration measurements and a model of vehicle drag. The concept was further developed to estimate aerodynamic flow angles in later papers, such as [4]. The proposed approach was validated using entry vehicle test flights on Earth, with known atmospheric conditions [5], and was subsequently applied to the reconstruction of the atmosphere of Mars based on measurements from the Viking entry probes [6]. Since Viking, the approach has been utilized on virtually every planetary atmospheric entry reconstruction to date. A recent thesis [7] documents the development and history of the algorithm, from its inception in the early 1960s to the most recent application of the method for the Mars Science Laboratory mission [8].

The previous approaches make use of measured accelerations and assumed aerodynamic models to solve for the freestream conditions by first computing density from the axial force coefficient and axial acceleration. The reconstructed density is then used to integrate the hydrostatic equation to estimate static pressure. The ratio of normal to axial and side to axial forces are then utilized to estimate the angles of attack and sideslip, respectively. The process can be iterated at each instant in time to improve the estimates; for instance, a combined inner and outer loop is implemented in [8] for solving the aerodynamic flow angles (inner loop) and freestream atmospheric conditions (outer loop). Note that the algorithm is completely deterministic in nature, although uncertainties in

American Institute of Aeronautics and Astronautics

the reconstructed quantities can be computed using linear covariance analysis techniques [7, 8]. Estimation of winds from the aforementioned methods has not been addressed directly; some approaches instead rely on a post-processing method such as that proposed in [9] for computing winds from flow angles and the navigation state.

Note that the methods described above have been implemented for post-flight reconstruction. The use vehicle aerodynamic models combined with data from an Inertial Measurement Unit (IMU) to provide real-time wind-relative state information to the vehicle guidance and control system has been proposed. Koifman and Bar-Itzhack [10] develop a Kalman filter approach for blending IMU data with an aircraft dynamic model for improved vehicle navigation, including wind velocity in the filter state. Colgren, Frye, and Olsen [11] develop a determinisic algorithm for estimating aerodynamic flow angles from IMU specific force measurements and an aircraft aerodynamic force model for the U-2 aircraft. Wise [12] introduces a Kalman filter method that uses body acceleration and Pitot tube measurements to estimate the aerodynamic flow angles for the X-45 Unmanned Combat Aerial Vehicle. This system is proposed as a backup system to air data vanes on the X-45. It is limited however in the need for Pitot airspeed measurements. McLaren [13] develops a method for airspeed estimation following an air data sensor failure that utilizes a Kalman filter to process IMU data and geometric relations to determine the wind vector. The method was successfully flight tested onboard a Calspan variable stability Learjet[14]. Reference [15] develops a deterministic algorithm for aerodynamic flow angle estimates that makes use of accelerometer measurements and a linearized aircraft aerodynamic model. Reference [16] proposes a Kalman filter method for blending wind forecast data, inertial measurement unit data, and and aircraft model for wind gust estimation. The method is proposed as a backup air data sensor for aircraft applications.

On-board blending of IMU data with vehicle aerodynamic models has also been proposed for entry vehicle applications. Westhelle [17] develops a deterministic algorithm using ratios of specific force measurements and an aerodynamic model for computing an estimate of the aerodynamic flow angles, dynamic pressure, and Mach number. The method is proposed as a backup air data system for the X-38 crew return vehicle. Lim, Pileggi, and Barton [18] develop a Bank-to-Steer control algorithm that utilizes the polarity of the commanded control torque to estimate the vehicle trim angle of attack for Apollo-class entry vehicles. Reference [19] develops a Kalman filter method for processing forecast wind data and accelerometer measurements to estimate wind gusts and aerodynamic flow angles during atmospheric entry. Estimates of density, dynamic pressure, and Mach number are not considered in [19].

A recently proposed model-based wind-relative state estimation method is a technique known as a Synthetic Air Data Sensing (SADS) system[20, 21, 22]. The SADS approach makes use of an aerodynamic model of the

vehicle, combined with acceleration and angular rate measurements on an onboard IMU to estimate the freestream aerodynamic and atmospheric conditions using a bank of Kalman filters. A SADS system can be used either as a backup, or as an alternative to a traditional FADS system that does not require pressure transducers. The past research on inertial based wind and angle of attack and sideslip estimation proves the viability of inertial measurements as a second source of air data information.

This paper extends the SADS concept[20] to the planetary probe entry vehicle atmosphere estimation problem. The method developed in this paper is similar to that of [20], in which a model of the vehicle dynamics is combined with an inertial navigation system to produce estimates of the atmospheric winds using a Kalman filter method for improved navigation and flight control. One important drawback of [20] is that the atmospheric density and pressure are not estimated in the filter; instead these are assumed to be known as a function of altitude. This assumption is not suitable for planetary probe entry estimation in which the atmospheric properties are highly uncertain. In this paper, the concept of atmospheric estimation aided by a vehicle aerodynamics model is extended to estimate freestream density and pressure in addition to winds. This new approach is developed for planetary entry atmospheric state estimation, and it is anticipated that the method can be applied to other applications such as high speed aircraft.

The remainder of this paper is organized as follows. Section II develops the synthetic air data system approach for entry vehicle atmosphere estimation using aerodynamic models and IMU measurement data. The approach is then applied to flight data from the Mars Science Laboratory (MSL) mission from August 2012 in Section III. The proposed method is compared to data from the MSL Entry, Descent, and Landing Instrumentation (MEDLI) project [23], which flew an array of pressure transducers on the MSL heatshield arranged as a FADS system to obtain data to be used for reconstruction the atmosphere and aerodynamics of the entry vehicle [24]. Section IV describes the potential use of the proposed method to augment the Mars 2020 Entry, Descent, and Landing Instrumentation (MEDLI2) project [25], which will fly a heatshield instrumented with pressure transducers with different full scale ranges to better capture the low pressure, supersonic flight regime at low altitudes. Only a single stagnation pressure measurement will be available during the high altitude, hypersonic flight regime. It is expected that the method proposed in this paper will augment the MEDLI2 dataset by providing some additional wind-relative state information during the hypersonic portion of flight where the single stagnation point measurement is available. A linear covariance analysis is conducted in Section IV to compare the proposed SADS estimates accuracy to the expected FADS performance under a common set of assumptions.

II. Atmospheric State Estimation

The approach for SADS-based state estimation proposed in this paper makes use of the state from the on-board navigation system combined with the vehicle aerodynamic database to estimate the atmospheric conditions. The estimation algorithm is aided by both a priori atmospheric models tabulated vs. altitude to be used as a pseudo measurement and initial guess at the atmosphere profile, and atmospheric models based on the hydrostatic equation that are integrated along the trajectory within the algorithm to propagate information forward in time from one measurement sample to the next.

A. Measurement Model

This work assumes that an aerodynamic model of the entry capsule is available, in which force and moment coefficients can be calculated from a given flight condition. It is assumed the aerodynamic model produces outputs in some known coordinate frame, such as that shown in Figure 1. Dimensional aerodynamic forces and moments acting on the vehicle are then computed using the relations
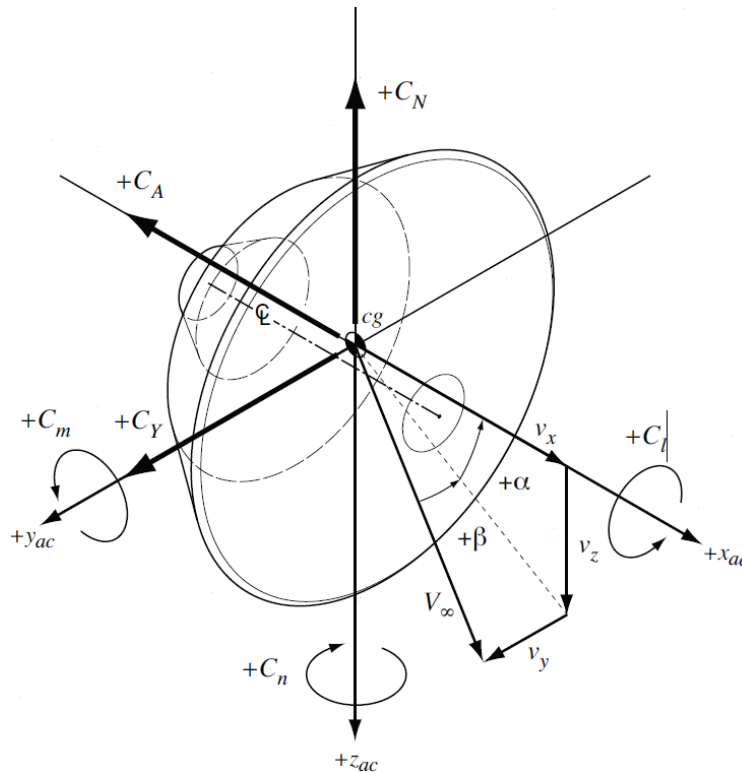
Figure 1. Body Coordinate System

$$\mathcal{F}(\boldsymbol{x}, \boldsymbol{u}) \quad = \quad m\boldsymbol{a} = \frac{1}{2}\rho V^2 S \left\{ \begin{array}{c} -C_A(\alpha, \beta, M, \boldsymbol{\lambda}) \\ C_Y(\alpha, \beta, M, \boldsymbol{\lambda}) \\ -C_Z(\alpha, \beta, M, \boldsymbol{\lambda}) \end{array} \right\} \tag{1}$$

$$\mathcal{M}(\boldsymbol{x}, \boldsymbol{u}) \quad = \quad \mathcal{I}\dot{\boldsymbol{\omega}} + \boldsymbol{\omega} \times \mathcal{I}\boldsymbol{\omega} = \frac{1}{2}\rho V^2 Sb \left\{ \begin{array}{c} C_l(\alpha, \beta, M, \boldsymbol{\lambda}) \\ C_m(\alpha, \beta, M, \boldsymbol{\lambda}) \\ C_n(\alpha, \beta, M, \boldsymbol{\lambda}) \end{array} \right\} \tag{2}$$

where $\boldsymbol{x} = [\rho, p_s, w_n, w_e, w_d]^{\mathsf{T}}$ is the atmospheric state, $\boldsymbol{\lambda}$ is a vector comprised of the aerodynamic database uncertainty factors, which are a collection of adders and multipliers used to perturb the aerodynamics, $\boldsymbol{u} = [\boldsymbol{\nu}, \boldsymbol{\lambda}]^{\mathsf{T}}$ are combined model parameters, and the vehicle planet-relative navigation state is $\boldsymbol{\nu} = [r, \Theta, \Lambda, v_n, v_e, v_d, \phi, \theta, \psi]^{\mathsf{T}}$.

Atmosphere model data can be incorporated into the state estimate as prior information. Atmosphere model data can be incorporated using table look-ups where the atmospheric conditions and uncertainties are tabulated as a function of altitude along some nominal trajectory. The model of this form produces an estimate of the atmospheric conditions, along with an associated error covariance matrix.

The aerodynamic force and moment and atmosphere models can be combined into a single expression,

$$\boldsymbol{z} = \boldsymbol{h}(\boldsymbol{x}, \boldsymbol{u}) = \left[\begin{array}{c} \mathcal{F}(\boldsymbol{x}, \boldsymbol{u}) \\ \mathcal{M}(\boldsymbol{x}, \boldsymbol{u}) \\ \boldsymbol{x} \end{array} \right] \tag{3}$$

Note that the measurement error covariance matrix $\boldsymbol{R}$ is a function of both sensor and mass property uncertainties.

B. Process Model

A model of the change in atmospheric conditions along the trajectory can be derived from basic idealized relations such as the hydrostatic equation and the perfect gas law. Such simplified relationships are suitable for implementation in the algorithm for propagating the atmospheric state estimate forward between aerodynamic measurements, which are assumed to occur at a reasonably high rate (several samples per second) along the trajectory. Since the simplified model involves idealized approximations, uncertainties in the model can be accounted for with process noise.

A model for the rate of change in static pressure can be found by rewriting the hydrostatic equation as the time derivative of pressure along a given trajectory, namely

$$\dot{p}_s = \rho g v_d \tag{4}$$

Similarly, a model for the rate of change in density along the trajectory can be derived from the perfect gas law, with the assumption that the atmosphere is locally isothermal ($\dot{T} \approx 0$) between measurement samples. The equation is of the form

$$\dot{\rho} = \frac{\dot{p}_s}{\Re T} = \frac{\dot{p}_s \rho}{p_s} = \frac{g v_d \rho^2}{p_s} \tag{5}$$

A reasonable simplified model for the rate of change in atmospheric winds is to assume a random walk model where the deterministic portion of the model is simply $\dot{w}_n = \dot{w}_e = \dot{w}_d = 0$. Thus, the process model can be written in the form

$$\dot{\boldsymbol{x}} = \boldsymbol{f}(\boldsymbol{x}, \boldsymbol{u}) + \boldsymbol{\eta} \tag{6}$$

where $\boldsymbol{\eta}$ is a process uncertainty term that is assumed to be zero mean with spectral density $\boldsymbol{Q}$, and

$$\boldsymbol{f}(\boldsymbol{x}, \boldsymbol{u}) = \left\{ \begin{array}{c} gv_d\rho^2/p_s \\ \rho g v_d \\ 0 \\ 0 \\ 0 \end{array} \right\} \tag{7}$$

The continuous model in Eq. (6) can be transformed to a discrete model of the form,

$$\boldsymbol{x}_{k+1} = \boldsymbol{x}_k + \boldsymbol{f}(\boldsymbol{x}_k, \boldsymbol{u}_k)\,\Delta t \tag{8}$$

which is suitable for propagation between measurements.

C. Data Fusion Algorithm

The atmospheric state estimate can be determined from a fusion of the available data sources, including the aerodynamic force and moment measurements, the prior tabulated data, and information from the process model. The proposed algorithm is in the form of an Iterated Extended Kalman-Schmidt Filter (IEKSF) [26] incorporating the process and measurement models described above. The IEKSF approach incorporates parameter uncertainties in the process and measurement models, thus producing a realistic state covariance estimate.

The algorithm is structured as a predictor-corrector method, in which state estimates are propagated between measurement samples using the relations

$$\bar{\boldsymbol{x}}_{k+1} = \hat{\boldsymbol{x}}_k + \boldsymbol{f}(\bar{\boldsymbol{x}}_k, \bar{\boldsymbol{u}}_k)\,\Delta t \tag{9}$$

$$\bar{\boldsymbol{P}}_{k+1} = \boldsymbol{\Phi}_k \hat{\boldsymbol{P}}_k \boldsymbol{\Phi}_k^{\mathsf{T}} + \boldsymbol{\Phi}_k \hat{\boldsymbol{C}}_k \boldsymbol{G}_k^{\mathsf{T}} + \boldsymbol{G}_k \boldsymbol{C}_k^{\mathsf{T}} \boldsymbol{\Phi}_k^{\mathsf{T}} + \boldsymbol{G}_k \boldsymbol{\Omega}_k \boldsymbol{G}_k^{\mathsf{T}} + \tilde{\boldsymbol{Q}}_k \tag{10}$$

$$\bar{\boldsymbol{C}}_{k+1} = \boldsymbol{\Phi}_k \hat{\boldsymbol{C}}_k + \boldsymbol{G}_k \boldsymbol{\Omega}_k \tag{11}$$

where $\boldsymbol{\Phi}_k$ is the state transition matrix and $\tilde{\boldsymbol{Q}}_k$ is the discrete-time process noise covariance. These quantities can be jointly calculated from the Van Loan matrix integral[27], given by

$$\exp\left(\begin{bmatrix} -\boldsymbol{F}_k & \boldsymbol{Q}_k \\ \boldsymbol{0} & \boldsymbol{F}_k \end{bmatrix}\Delta t\right) = \begin{bmatrix} \boldsymbol{X}_{11} & \boldsymbol{X}_{12} \\ \boldsymbol{0} & \boldsymbol{X}_{22} \end{bmatrix} = \begin{bmatrix} \boldsymbol{X}_{11} & \boldsymbol{\Phi}_k^{-1}\tilde{\boldsymbol{Q}}_k \\ \boldsymbol{0} & \boldsymbol{\Phi}_k^{\mathsf{T}} \end{bmatrix} \tag{12}$$

which leads to the result $\boldsymbol{\Phi}_k = \boldsymbol{X}_{22}^\mathsf{T}$ and $\tilde{\boldsymbol{Q}}_k = \boldsymbol{\Phi}_k \boldsymbol{X}_{12}$. Assuming a reasonably fast integration step (1 Hz or higher), these quantities can be approximated by $\boldsymbol{\Phi}_k \approx \boldsymbol{I} + \boldsymbol{F}_k \Delta t$ and $\tilde{\boldsymbol{Q}}_k \approx \boldsymbol{Q}_k \Delta t$.

Due to measurement equation nonlinearity, the measurement update step is an iterative process to solve a nonlinear least squares regression problem, involving the measurement and the state prediction as observations. The process is given by the equations

$$\boldsymbol{S}_{k,i} = \boldsymbol{H}_{k,i}\bar{\boldsymbol{P}}_{k,i}\boldsymbol{H}_{k,i}^\mathsf{T} + \boldsymbol{H}_{k,i}\bar{\boldsymbol{C}}_k\boldsymbol{L}_k^\mathsf{T} + \boldsymbol{L}_k\bar{\boldsymbol{C}}_k^\mathsf{T}\boldsymbol{H}_{k,i}^\mathsf{T} + \boldsymbol{R}_k \tag{13}$$

$$\boldsymbol{K}_{k,i} = \left[\bar{\boldsymbol{P}}_k\boldsymbol{H}_{k,i}^\mathsf{T} + \bar{\boldsymbol{C}}_k\boldsymbol{L}_k^\mathsf{T}\right]\boldsymbol{S}_{k,i}^{-1} \tag{14}$$

$$\hat{\boldsymbol{x}}_{k,i+1} = \bar{\boldsymbol{x}}_k + \boldsymbol{K}_{k,i}\left[\boldsymbol{z}_k - \boldsymbol{h}\left(\hat{\boldsymbol{x}}_{k,i}, \boldsymbol{u}_k\right) - \boldsymbol{H}_{k,i}\left(\bar{\boldsymbol{x}}_k - \hat{\boldsymbol{x}}_{k,i}\right)\right] \tag{15}$$

Equations (13)–(15) are iterated until convergence or until reaching a prescribed iteration limit. After the iteration is complete, the state covariance and state-parameter covariance matrices can be computed as

$$\hat{\boldsymbol{P}}_k = \bar{\boldsymbol{P}}_k - \boldsymbol{K}_k\boldsymbol{S}_k\boldsymbol{K}_k^\mathsf{T} \tag{16}$$

$$\hat{\boldsymbol{C}}_k = \bar{\boldsymbol{C}}_k - \boldsymbol{K}_k\left[\boldsymbol{H}_k\bar{\boldsymbol{C}}_k + \boldsymbol{L}_k\boldsymbol{\Omega}_k\right] \tag{17}$$

The IEKSF method has the advantage of providing optimal state estimates that account for systematic parameter uncertainties to produce a realistic state covariance estimate.

D. Aerodynamic State Transformations

The atmospheric state (winds, pressure, and density) are outputs of the proposed SADS data processing algorithm. The atmospheric state can readily be combined with the INS state solution to produce estimates of aerodynamic states, including angle of attack, sideslip, Mach number, and dynamic pressure. Uncertainties can be mapped from the atmospheric and INS states into the aerodynamic states through linear covariance analysis. The equations of the transformation from atmospheric and INS states to aerodynamic states are readily available in various sources such as [28] and are not repeated here.

III. Application to Mars Science Laboratory

On August 5th 2012, the Mars Science Laboratory (MSL) entry vehicle successfully entered the atmosphere of Mars and landed the Curiosity rover safely on the surface of the planet in Gale crater. The MSL entry vehicle was comprised of a 70-degree sphere-cone heatshield and backshell consisting of a stack of three truncated cones. The MSL vehicle as-built outer mold line is shown in Figure 2(a) [29]. During most of entry, the capsule used a radial

center of mass offset to fly at an angle of attack (approximately 16 degrees at hypersonic conditions). This attitude produced lift to fly a guided entry profile, reducing the landing footprint to a much smaller size than any previous Mars mission. To fly the guided entry, the vehicle carried four pairs of Reaction Control System (RCS) jets to perform maneuvers and damp rates. The four pairs of jets could be fired rapidly in different combinations to provide control torque about any axis by modulating the pulses of the jet.

(a) As Built MSL Outer Mold Line

(b) MEDLI/MEADS Geometry (Looking Aft)
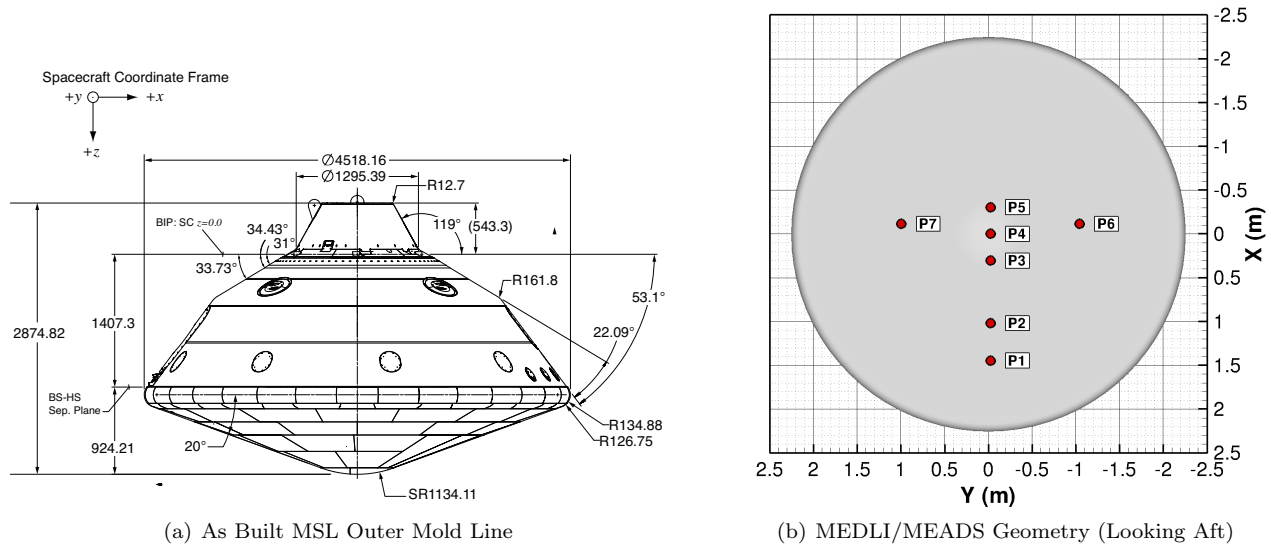
Figure 2. Vehicle Geometry

MSL carried with it an instrumentation package designed to measure the aerodynamic and aerothermal environments during atmospheric entry. This instrumentation package was known as the MSL Entry, Descent, and Landing Instrumentation (MEDLI) [23], which consisted of three major subsystems: the Mars Entry Atmospheric Data System (MEADS), the MEDLI Integrated Sensor Plugs (MISP), and the Sensor Support Electronics (SSE). The MEADS consisted of seven pressure transducers connected to flush orifices in the heat shield to measure pressures across the vehicle forebody. The MISP devices were a system of seven thermocouple and recession sensors that provided aerothermal measurements of the heat shield performance. The SSE provided power to the sensors, conditioned their signals, and transmitted the data to storage on the Curiosity rover. The MEDLI sensors provided measurements that were used for trajectory reconstruction and engineering validation of aerodynamic, atmospheric, and thermal protection system models in addition to Earth-based systems testing procedures. The MEDLI data and its usage for reconstructing the aerodynamic and aerothermal performance of the MSL entry vehicle are described in [30, 31, 32].

The remainder of this section is focused on the application of the SADS method developed in the previous section

to flight data obtained from the MSL mission. The SADS-based estimates can be compared to the reconstructed atmosphere based on the MEDLI flight data [30], providing a useful check case in the form of an air data system that used data from calibrated pressure transducers [33].
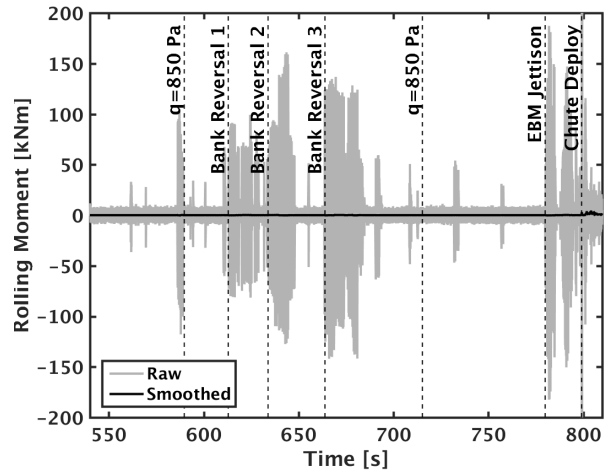
The aerodynamic forces and moments were sensed by the on-board IMU in the form of acceleration and angular rate measurements at a frequency of 200 Hz. The dimensional aerodynamic forces and moments were calculated from these measurements and mass property models of the vehicle. Forces and moments due to the RCS firing were subtracted from the total force and moment measurements. The results were found to be sensitive to vibration and noise associated with RCS firings, so a low-pass optimal Fourier smoother with a cut-off frequency of 2 Hz was applied to smooth the data [31]. Note that the smoother that was implemented in these results was done so in a way that mimiced on-board computation, so artifacts such as lags are introduced. The raw and smoothed aerodynamics are shown in Figure 3. Note the increase in noise around the time of bank reversals, which correlate with the times of RCS thruster commands shown in Figure 4. The smoothed side/normal and pitch/yaw moments are shown in Figure 5.

The SADS filter was initialized at 580 s in the MSL EDL timeline, corresponding to an altitude of approximately 66.15 km. The filter was implemented to run at a rate of 64 Hz to match the rate of the on-board navigation state. The filter was terminated at a time of 800 s, at an altitude of 7.10 km. The SADS filter was set to use a maximum of 10 iterations at each measurement sample. Convergence of the solution was said to occur if the norm of the difference between state estimates at subsequent iterations divided by the current estimate was less than 10^{-6}. Given the sensitivity of moments to the RCS noise, the filter was set to ignore moment measurements while the RCS was active and rely solely on force measurements. The filter made use of the post-flight reconstructed aerodynamic model described in [31] as a means to directly compare FADS and SADS given consistent data sources. Uncertainties in the aerodynamic database were based on those provided in [34]. The initial atmospheric state and the prior atmosphere tables were based on pre-flight mesoscale models [35]. The initial atmospheric state and table data covariance is based on the uncertainty analysis performed by the atmospheric scientists who developed the model, and no tuning of these uncertainties was performed. The prior atmosphere table and the associated uncertainties are shown in Figure 6. Note that the mesoscale model does not produce an uncertainty estimate for static pressure, and so it was assumed here that the static pressure uncertainty percentage was equal to that corresponding to density. The mesoscale model downward wind component was assumed to be zero with a 3σ uncertainty of 7.5 m/s.
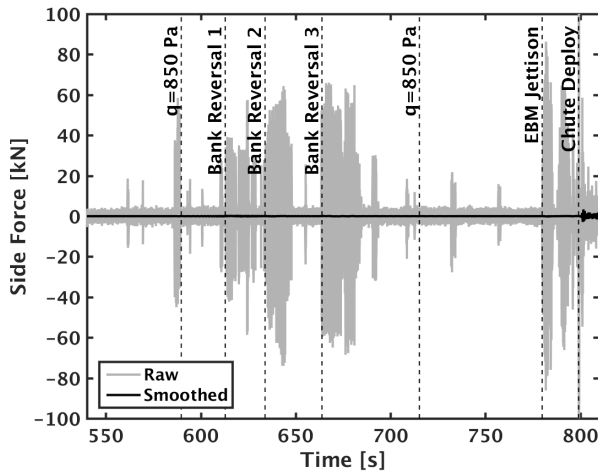
Components of the process model spectral density were tuned using preflight simulation data to encapsulate the
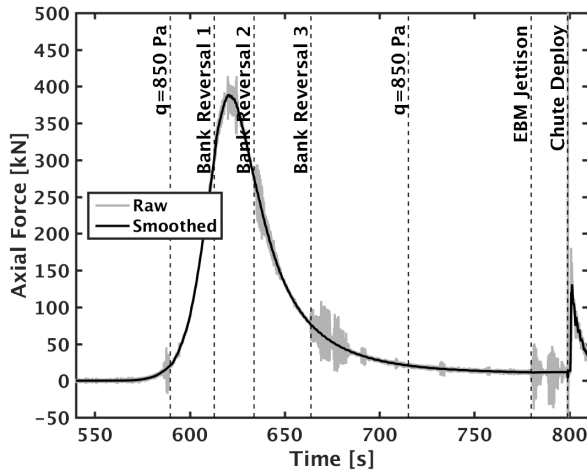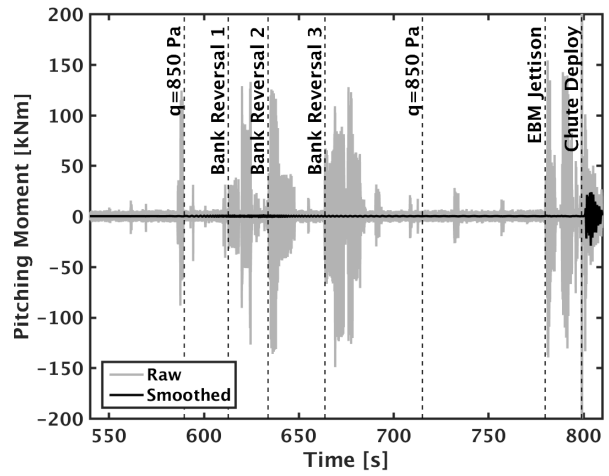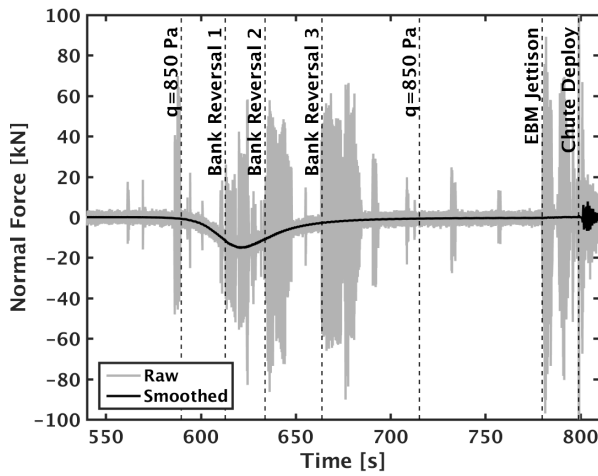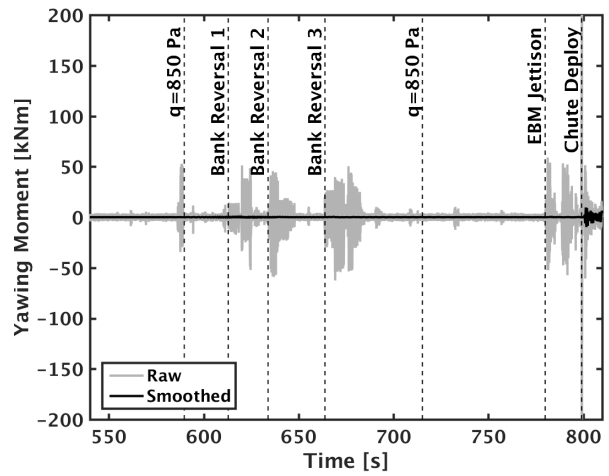
(a) Axial Force

(b) Rolling Moment

(c) Side Force

(d) Pitching Moment

(e) Normal Force

(f) Yawing Moment
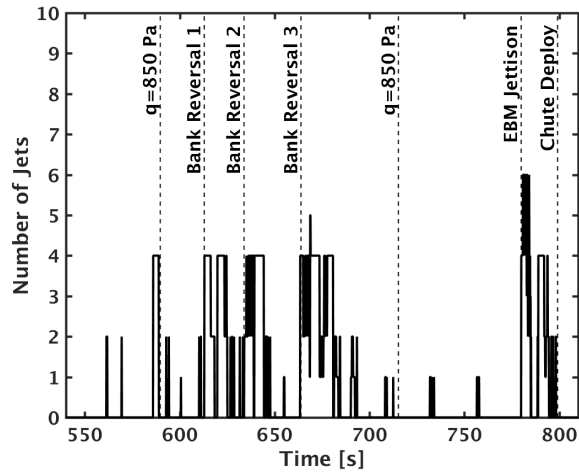
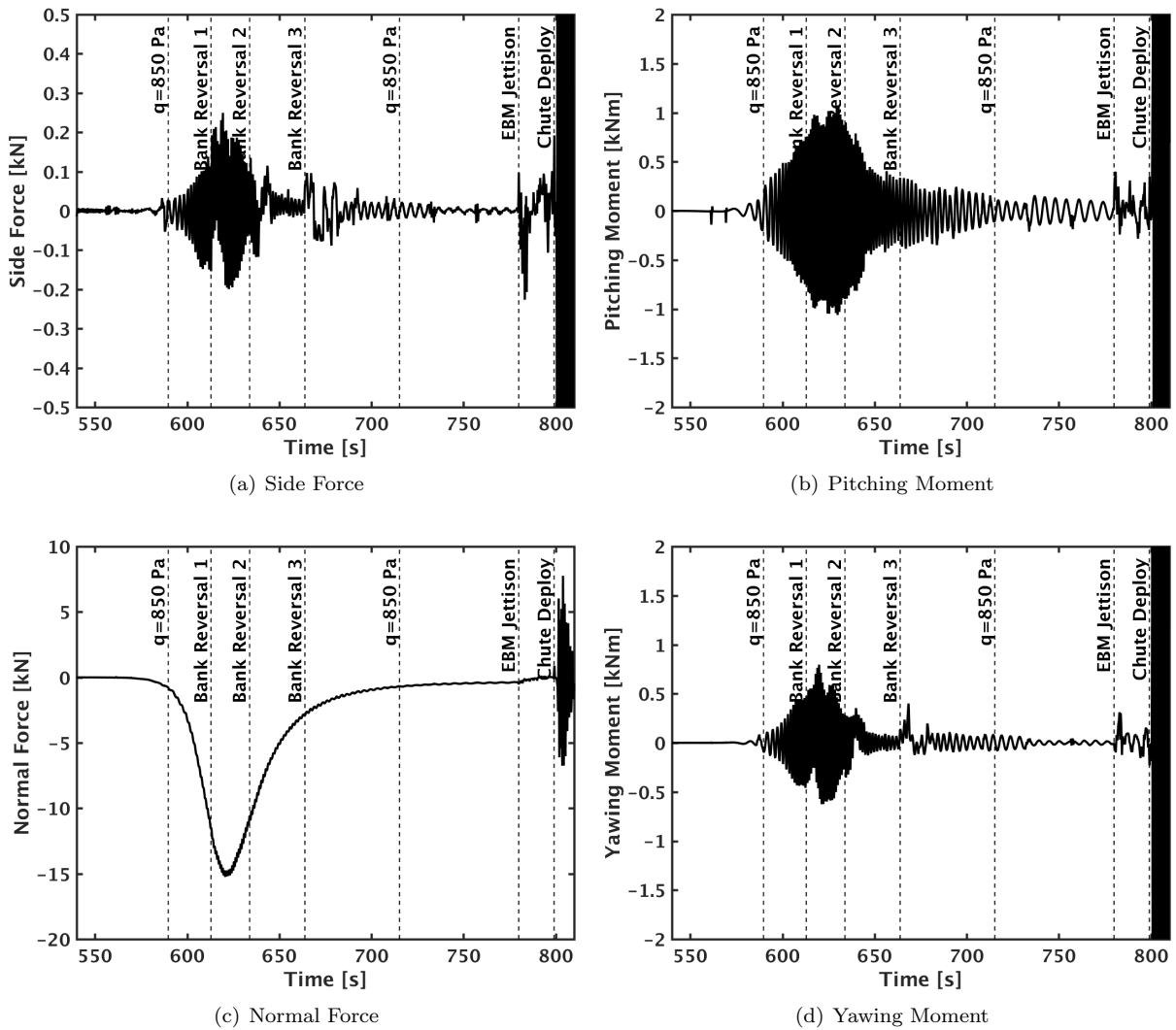Figure 3. Measured Aerodynamic Forces and Moments

Figure 4. RCS Firing

(a) Side Force

(b) Pitching Moment

(c) Normal Force

(d) Yawing Moment

Figure 5. Smoothed Aerodynamic Forces and Moments

(a) Mesoscale Atmosphere

(b) Mesoscale Winds

(c) Mesoscale Uncertainties
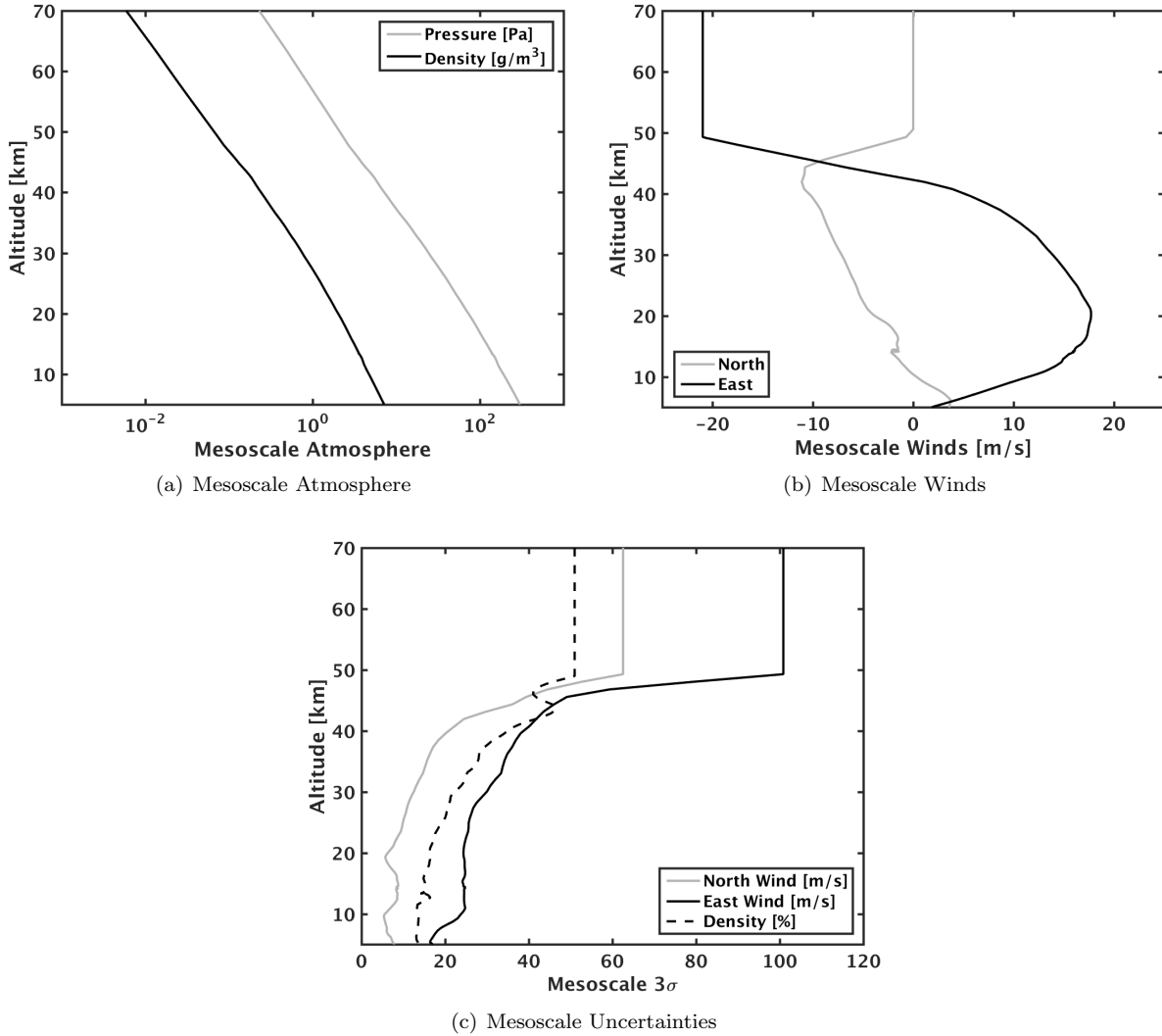
Figure 6. Mesoscale Atmosphere and Uncertainties

maximum range of expected deviations in the between the hydrostatic assumption compared to the mesoscale model for this class of trajectory. The 3σ density process model uncertainty was set to 20%/s at the initial altitude of 66.15 km, and was scaled linearly to 1%/s at the altitude of 13.5 km (650 s in the MSL EDL timeline) and then held constant. The 3σ pressure process model uncertainty was held constant over entire trajectory at a value of 0.01%/s. The 3σ components corresponding to the horizontal winds were set to a constant value of 35 m/s^2, and the 3σ downward wind component was 8.5 m/s^2.

Results of the SADS filter are shown in the following figures. The results are compared to true air data estimation results from the MEADS pressure measurement data, described in [36]. In the following figures, the pressure transducer-based estimation is labeled FADS, and new synthetic air data solution developed in this paper is labeled as SADS.
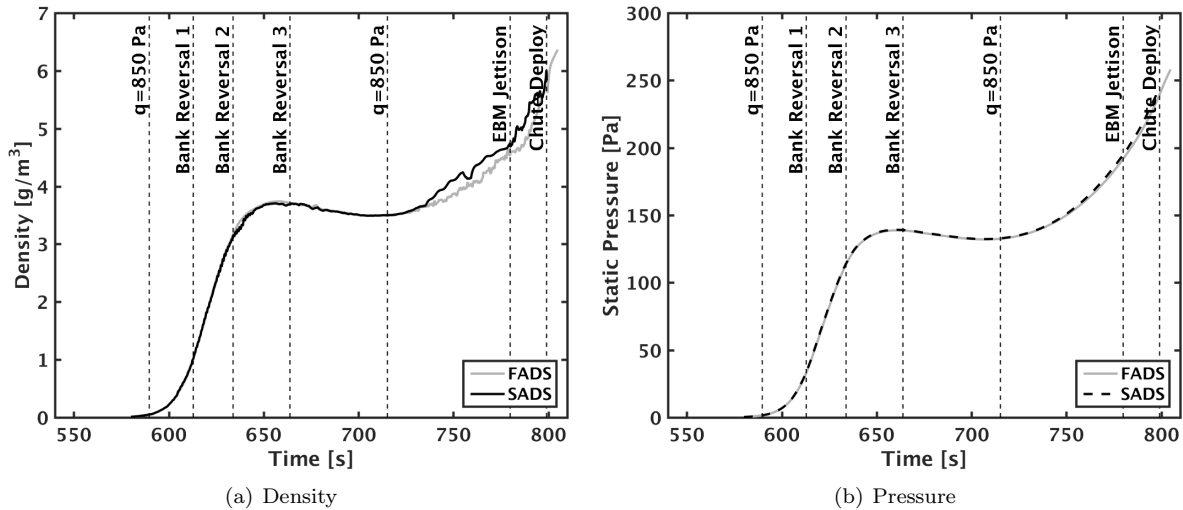
(a) Density

(b) Pressure

Figure 7. Atmosphere

The atmospheric density and pressure estimates are shown in Figure 7. The two solutions give consistent results. Some differences are apparent in the low supersonic flight regime, below 850 Pa dynamic pressure. These differences are consistent with those between the post-flight reconstructed axial force coefficient and the reconciled aerodynamics, as described in [31]. These differences are attributable to transducer instrumentation errors in low pressure ranges that are outside their design requirements. Differences in density and pressure estimates are within 0.5% over the range in which the transducers were calibrated (above 850 Pa dynamic pressure).

The estimated winds along the trajectory are shown in Figure 8. The two methods produce consistent estimates, although the SADS exhibits more noise in the estimate. The noise is likely due to vibrations in the accelerometer and smoothing artifacts not accounted for in the filter gain. The mean profile and general trends follow the FADS solution. This result is important as it indicates the ability of the SADS approach to mimic a true FADS system without the use of pressure sensors. The reconstructed winds from these two methods are consistent with observed vehicle dynamics and guidance response [37, 38]. Specifically, in [37] it was noted that the vehicle response during the third bank reversal was consistent with a roughly 10 m/s cross wind, blowing north to south, which matches with the northerly wind component calculated from both the FADS and SADS methods. Additionally, the time between entry balance mass jettison and parachute deployment was theorized in [38] to be due to a roughly 20 m/s tail wind, blowing to the east. This wind also matches with both the FADS and SADS estimates near the time of parachute deployment.

The dynamic pressure and Mach estimates are shown in Figure 9. The methods are in agreement over the entry
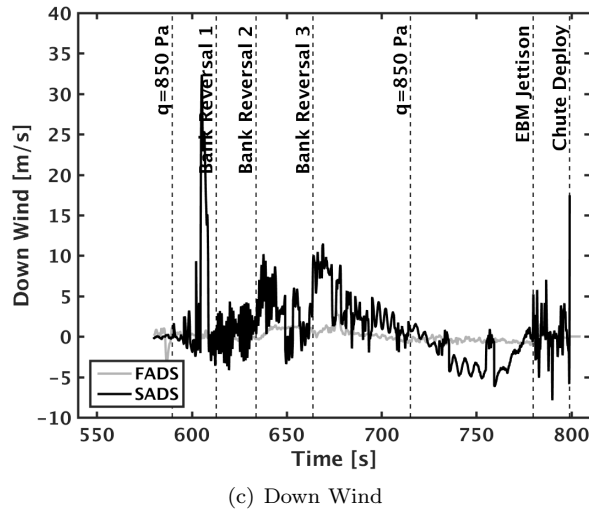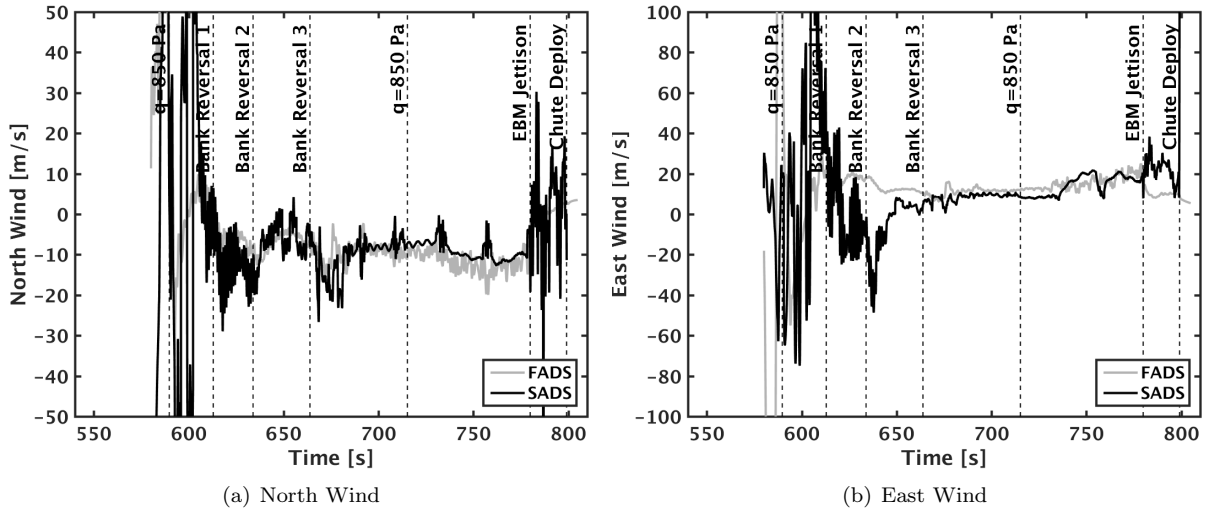
(a) North Wind

(b) East Wind

(c) Down Wind

Figure 8. Winds
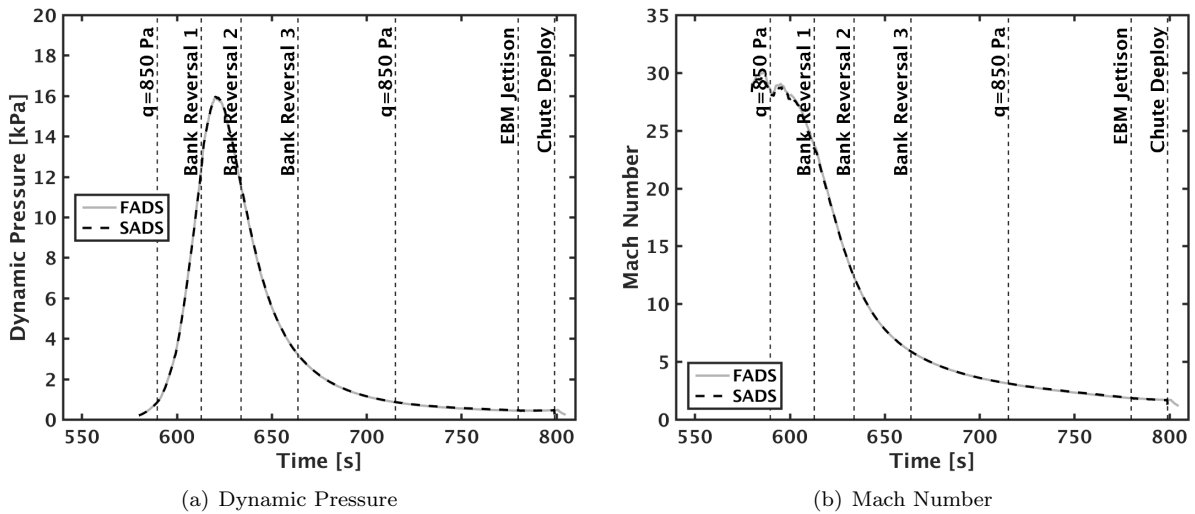

(a) Dynamic Pressure

(b) Mach Number

Figure 9. Dynamic Pressure and Mach Number

trajectory. Differences in the dynamic pressure and Mach estimates are on the order of 0.5% and 0.05, respectively, in region where the pressure measurements were calibrated. The aerodynamic flow angle estimates are shown in Figure 10. The FADS and SADS solutions are in agreement, with differences within 0.25 deg, thus indicating the SADS method is able to provide an estimate of the vehicle state that is consistent with a true air data system.

(a) Angle of Attack

(b) Angle of Sideslip
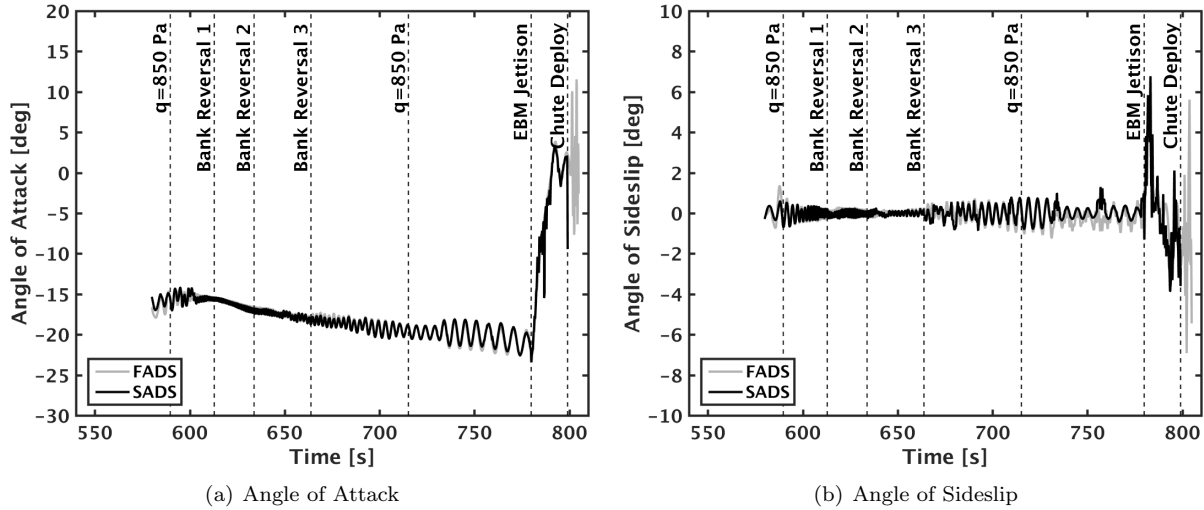
Figure 10. Aerodynamic Angles

IV. Application to the Mars 2020 Mission

Another MEDLI-like system of instruments is planned to be flown on the Mars 2020 mission. This instrumentation system, known as MEDLI2 [25], will acquire FADS pressure data to be used for the reconstruction of atmospheric states and vehicle aerodynamics during entry. The focus of the pressure system on MEDLI2 is geared toward estimating aerodynamics in the supersonic regime of flight, where some questions remain regarding the aerodynamic reconstruction of MSL [31]. To this end, the forebody pressure system will carry one transducer with a full scale range of 35 kPa (the same as MSL transducers) to measure stagnation pressure over the entire entry trajectory (which in turn yields estimates of dynamic pressure and density), and six transducers with a full scale range of 7 kPa to more accurately measure the atmosphere and aerodynamics in the supersonic regime of flight (roughly Mach 6 and below). In addition, one transducer will be installed on the backshell to measure the base pressure and its contribution to drag. The forebody pressure port layout corresponding to the current MEDLI2 design is shown in Figure 11. Note that port P1 corresponds to the hypersonic pressure transducer.

Since the focus of this instrumentation is on supersonic measurements, only one hypersonic transducer is available to provide estimates of the atmospheric conditions during entry for a large altitude range before the supersonic
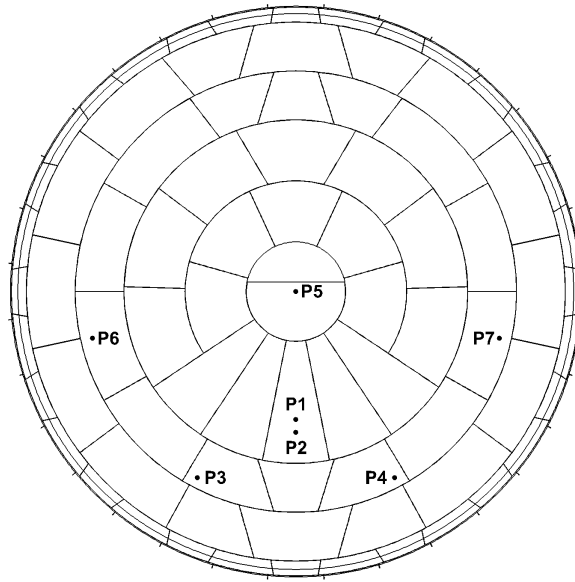
Figure 11. Mars 2020 Pressure Port Arrangement

transducers de-saturate at 7 kPa. The hypersonic stagnation pressure transducer will provide estimates of density

and dynamic pressure but will yield little to no information about the wind environment. It is anticipated that

the algorithm developed in this paper can augment the single pressure measurement to provide estimates of winds

along with a redundant estimate of density and dynamic pressure. The atmospheric states reconstructed from

this algorithm can also be used to initialize the filter that processes the supersonic pressure measurements as the

transducers de-saturate. Furthermore, the algorithm can serve as a backup in the event of supersonic transducer
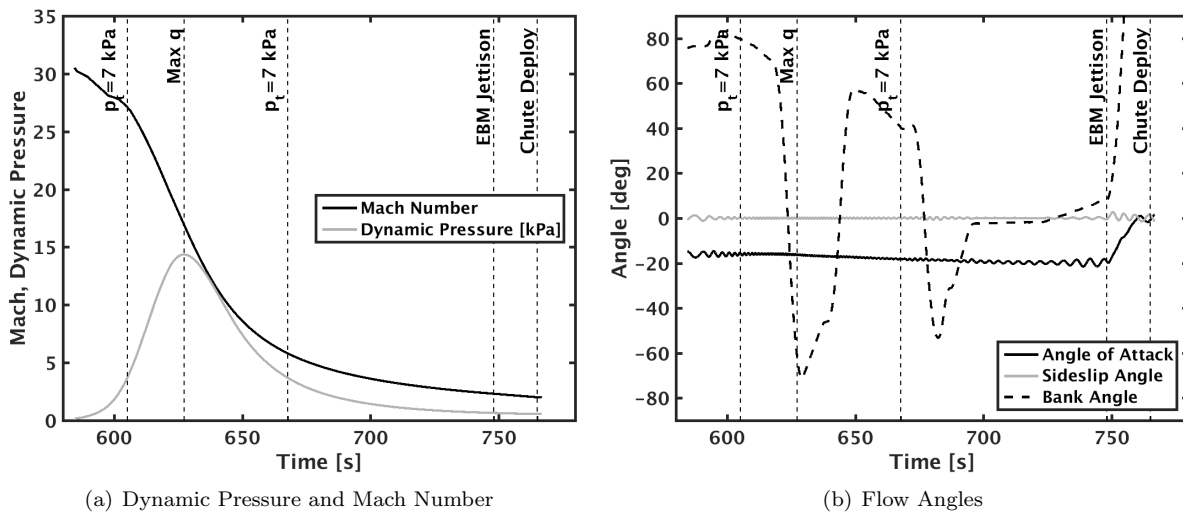
failures or anomalies.

(a) Dynamic Pressure and Mach Number

(b) Flow Angles

**Figure 12. Mars 2020 Reference Trajectory**

The following figures show the results of a linear covariance analysis of the synthetic air data sensing algorithm applied to a representative Mars 2020 entry trajectory. The reference trajectory used for this analysis is shown in Figure 12. Note that the supersonic FADS measurements are saturated over the time period from 605 s to 668 s. The synthetic air data method is compared against results of a single pressure port FADS air data estimate from the stagnation pressure port in the hypersonic flight regime, and a complete array of six pressure measurements in the supersonic regime. To stress the estimators, large a priori atmosphere uncertainties are used for this analysis, consisting of 50% uncertainty in density and pressure, 100 m/s in horizontal winds and 25 m/s in downward winds (all specified at the 3σ level). The process model uncertainties from the previous section are increased by an order of magnitude. The increased uncertainties on the prior atmosphere estimate and the process model have the effect of pushing the burden of algorithm onto the measurement model, thereby allowing a more direct comparison of the FADS vs. SADS measurements. The IMU model is based on the MSL flight hardware as described in [30]. The FADS pressure sensor are modeled with a non-repeatability uncertainty of 0.05% full scale pressure, and a noise floor of 30 Pa. Hysteresis uncertainties are included as a time-varying zero offset, modeled as random walk. The random walk uncertainty model was tuned to produce zero offsets on the order 30 Pa over the duration of the entry, based on transducer performance observed from MSL flight data.

Results of the linear covariance analysis of the two methods are shown in Figure 13. These results compare reconstructions of density, pressure, dynamic pressure, and Mach number. These results show that the SADS solutions produce estimates of density and dynamic pressure with higher uncertainties than the FADS algorithm. The incorporation of the hydrostatic process model enables the SADS estimator to produce estimates of static pressure that are similar to that of the FADS state estimator, although slightly less precise. A similar trend appears in the Mach number estimate uncertainty.

A comparison of the wind estimate uncertainties is shown in Figure 14. The SADS estimates provide some enhancement of the wind estimates during the hypersonic flight regime where the low scale supersonic pressure sensors are saturated. This effect is most noticeable in the north component, which is essentially a cross wind for this entry trajectory. The single hypersonic transducer provides estimates similar to the SADS method for the east (headwind) component. The FADS estimates are superior in all components in supersonic flight regime, where all pressure measurements are utilized. Note that the uncertainties in the SADS estimate of the downward wind component are weakly observable for this particular trajectory, as indicated by the uncertainties staying near to the a priori atmospheric uncertainties. This result is due to the high uncertainties in the aerodynamic database itself, which
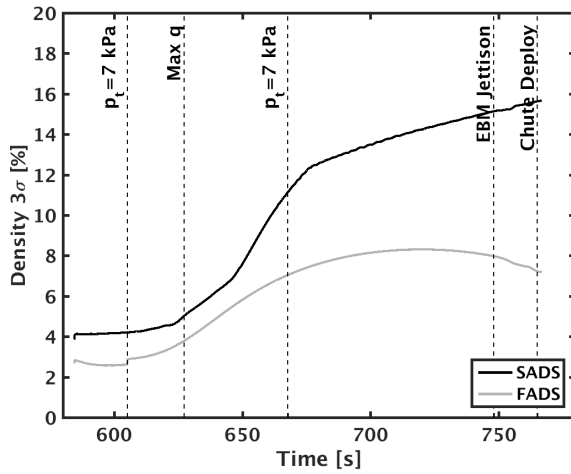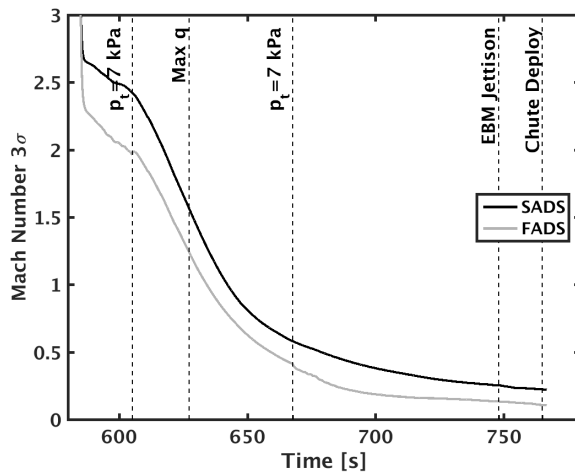
(a) Density
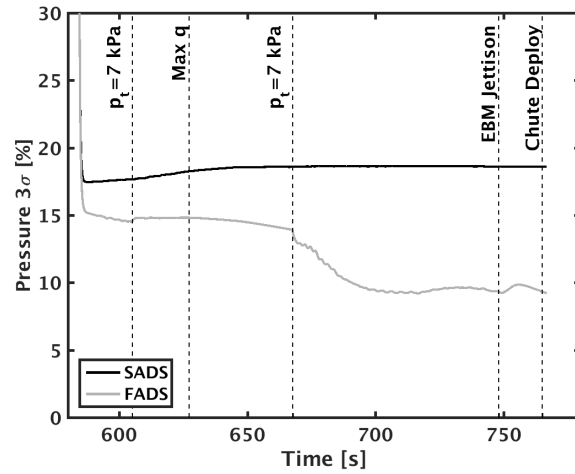
(b) Pressure
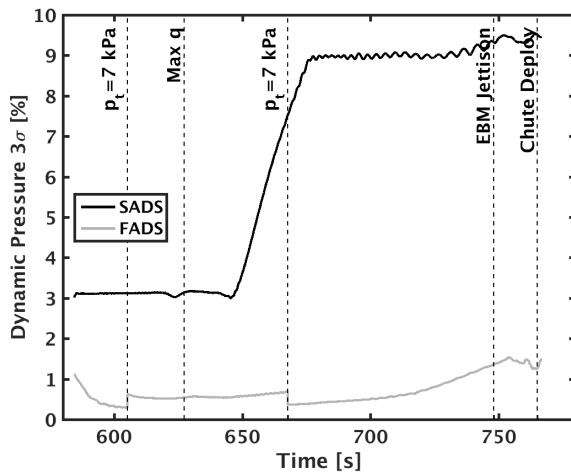
(c) Dynamic Pressure

(d) Mach Number

Figure 13. Comparison Between SADS and FADS - Density, Pressure, Dynamic Pressure, and Mach Number Uncertainties
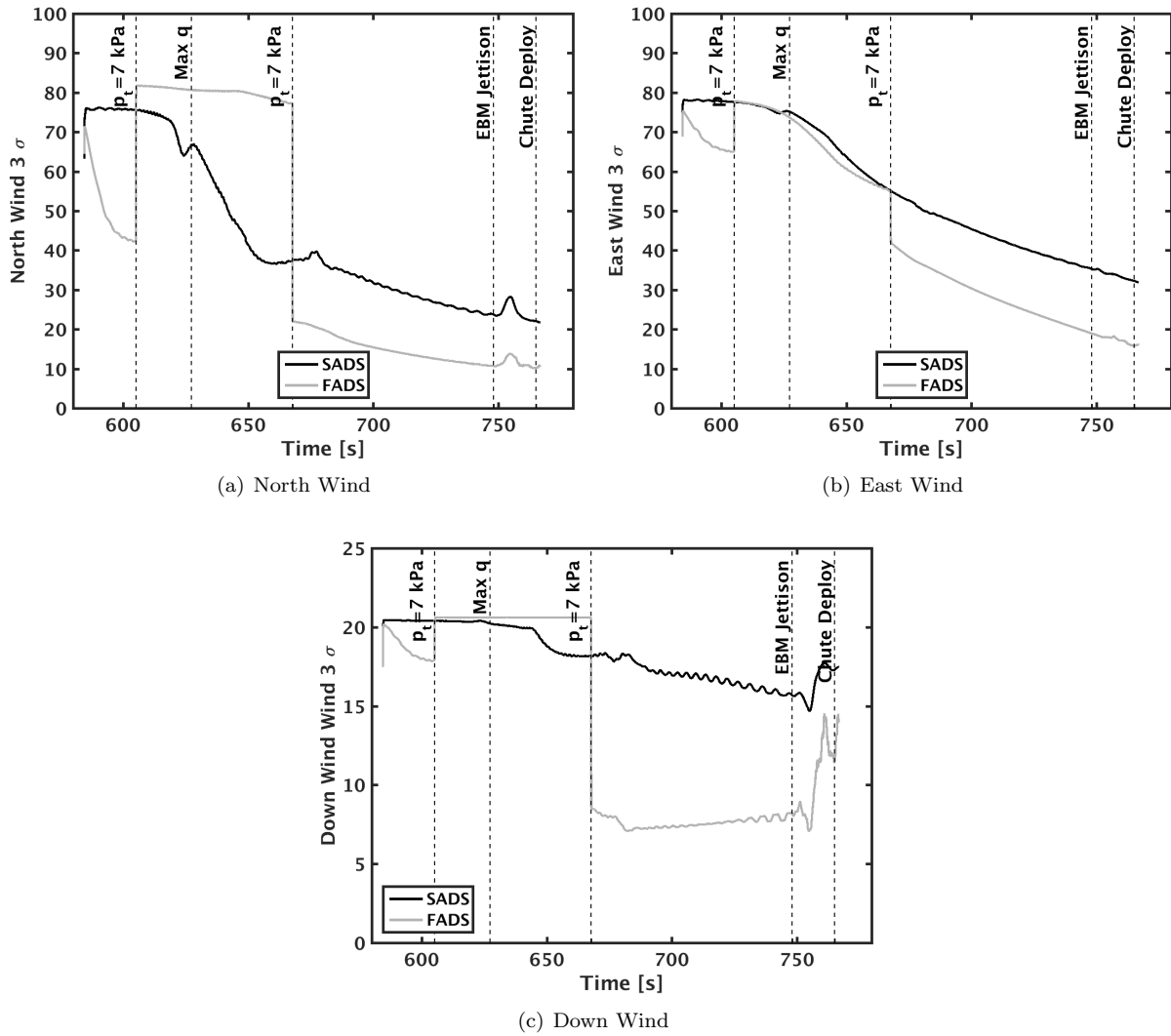
(a) North Wind

(b) East Wind

(c) Down Wind

Figure 14. Comparison Between SADS and FADS - Wind Uncertainties

American Institute of Aeronautics and Astronautics

obfuscates the effects horizontal vs. vertical winds in the measurement weighting. For these class of trajectories, it may be beneficial to remove the downward wind component as a filter state. Other classes of trajectories may have better observability of downward wind states.
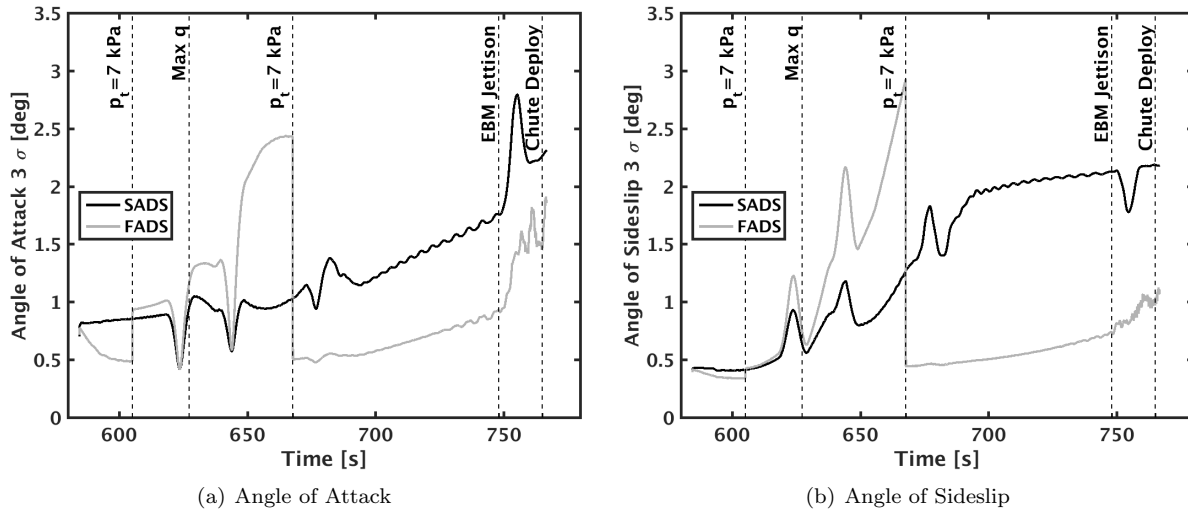

(a) Angle of Attack   (b) Angle of Sideslip

Figure 15. Comparison Between SADS and FADS - Flow Angle Uncertainties

Similar trends are evident in the aerodynamic flow angle uncertainties, shown in Figure 15. The SADS approach can improve on the FADS results during the period where the supersonic pressure transducers are saturated. The FADS method using all pressure transducers is far superior in the supersonic flight regime. The high uncertainties in the SADS estimates is due to the fact that the aerodynamic database uncertainties are highest in the supersonic flight regime.

V. Conclusions

An estimator suitable for planetary probe entry atmosphere estimation has been developed. This estimator is based on an aerodynamic database (forces and moments) combined with in-flight measurements of the vehicle aerodynamics computed from inertial measurement unit data (accelerations and rates). The atmospheric states (winds, density, and pressure) are estimated using a nonlinear Kalman-Schmidt filter approach in which the inertial state of the vehicle (position, velocity, and attitude) are assumed to be known from the navigation system, and the atmosphere states are solved for from the measured aerodynamic forces and moments. A test case with flight data from the Mars Science Laboratory mission shows that the method performs well and is consistent with atmosphere states independently estimates from a flush air data system.

The method is expected to be utilized to aid the Mars 2020 entry air data system by providing additional data

American Institute of Aeronautics and Astronautics

during periods in which the low pressure range transducers are saturated (above 7 kPa). Linear covariance analysis indicates that the synthetic method produces air data estimates with higher uncertainties than a true flush air data sensing system. Although the uncertainties in the derived atmosphere using the assumed aerodynamic model are higher than those computed from a traditional flush air data system, the proposed method provides an alternative for atmosphere estimation that does not require pressure transducers.

References

[1] Adler, M., Wright, M., Campbell, C., Clark, I., Engelund, W., and Rivellini, T., "Entry, Descent, and Landing Roadmap: Technology Area 09," NASA, April 2012.

[2] Dwyer Cianciolo, A. and Powell, R., "Entry, Descent, and Landing Guidance and Control Approaches to Satisfy Mars Human Mission Landing Criteria," American Astronautical Society, AAS Paper 17-254, February 2017.

[3] Seiff, A., "Possibilities for Determining the Characteristics of the Atmospheres of Mars and Venus from Gas-Dynamic Behavior of a Probe Vehicle," NASA TN D-1770, 1963.

[4] Nier, A. P., Hanson, W. B., McElroy, M. B., Seiff, A., and Spencer, N. W., "Entry Science Experiments for Viking 1975," *Icarus*, Vol. 16, 1972, pp. 74–91.

[5] Seiff, A., Reese, D. E., Sommer, S. C., Kirk, D. B., Whiting, E. E., and Neimann, H. B., "PAET, An Entry Probe Experiment in the Earth's Atmosphere," *Icarus*, Vol. 18, 1973, pp. 525–563.

[6] Seiff, A., "The Viking Atmospheric Structure Experiment - Techniques, Instruments, and Expected Accuracies," *Space Science Instrumentation*, Vol. 2, 1976, pp. 381–423.

[7] Kutty, P., "Reconstruction and Uncertainty Quantification of Entry, Descent and Landing Trajectories Using Vehicle Aerodynamics," M. S. Thesis, School of Aerospace Engineering, Georgia Institute of Technology, May 2014.

[8] Kutty, P. and Karlgaard, C. D., "Mars Science Laboratory Aerodatabase Trajectory Reconstruction and Uncertainty Assessment," AIAA Paper 2014-1094, January 2014.

[9] Kelly, G. M., Findlay, J. T., and Compton, H. R., "Shuttle Subsonic Horizontal Wind Estimation," *Journal of Spacecraft and Rockets,* Vol. 20, No. 4, 1983, pp. 390–397.

[10] Koifman, M. and Bar-Itzhack, I. Y., "Inertial Navigation System Aided by Aircraft Dynamics," *IEEE Transactions on Control Systems Technology*, Vol. 7, No. 4, 1999, pp. 487–493.

[11] Colgren, R. D., Frye, M. T., and Olsen, W. M., "A Proposed System Architecture for Estimation of Angle-of-Attack and Sideslip Angle," AIAA Paper 99-4078, 1999.

[12] Wise, K. A., "Flight Testing of the X-45A J-UCAS Computational Alpha-Beta System," AIAA Paper 2006-6215, August 2006.

[13] McLaren, S. A., "Velocity Estimate Following Air Data System Failure," M. S. Thesis, Department of Aeronautics and Astronautics, Air Force Institute of Technology, March 2008.

[14] McLaren, S. A., Beaverson, C. A., Sreeram, J., Powers, D. W., and Rothermel, W. H., "Back Up Velocity Estimate Following Air Data System Failure," Air Force Flight Test Center, Report AFFTC-TIM-07-09, December 2007.

[15] Myschik, S., Holzapfel, F., and Sachs, G., "Low-Cost Sensor Based Integrated Airdata and Navigation System for General Aviation Aircraft," AIAA 2008-7423, August 2008.

[16] Nebula, F., Palumbo, R., and Morani, G., "Virtual Air Data: a Fault-Tolerant Approach Against ADS Failures," AIAA Paper 2013-4568, August 2013.

[17] Westhelle, C. H., "X-38 Backup Air Data System," AIAA Paper 2002-0007, January 2002.

[18] Lim S., Pileggi, R., and Barton, G., "MIMO Adaptive Bank-To-Steer Control Algorithms for Guided Re-entry Vehicles," AIAA Paper 2007-6431, August 2007.

[19] Nebula, F., Palumbo, R., Morani, G., and Carraro, F., "Virtual Air Data System Architecture for Space Reentry Applications," *Journal of Spacecraft and Rockets*, Vol. 46, No. 4, 2009, pp. 818–828.

[20] Lie, F. and Gebre-Egziabher, D., "Synthetic Air Data System," *Journal of Aircraft*, Vol. 50, No. 4, 2013, pp. 1234–1249.

[21] Lie, F., "Synthetic Air Data System: A Case Study of Model-Aided Estimation," Ph.D. Dissertation, Department of Aerospace Engineering and Mechanics, University of Minnesota, September 2014.

[22] Lie, F. and Gebre-Egziabher, D., "Sensitivity Analysis of Model-Based Synthetic Air Data Estimators," AIAA Paper 2015-0081, January 2015.

[23] Munk, M. M., Little, A., Kuhl, C., Bose, D., and Santos, J., "The Mars Science Laboratory (MSL) Entry, Descent, and Landing Instrumentation (MEDLI) Hardware," AAS Paper 13-310, February 2013.

[24] Cheatwood, F. M., Bose, D., Karlgaard, C., Kuhl, C. A., Santos, J. A., and Wright, M. J., "Mars Science Laboratory (MSL) Entry, Descent, and Landing Instrumentation (MEDLI): Complete Flight Data Set," NASA TM-2014-218533, October 2014.

[25] Hwang, H., Bose, D., White, T., Wright, H., Schoenenberger, M., Kuhl, C., Trombetta, D., Santos, J., Oishi, T., Karlgaard, C., Mahzari, M., and Pennington, S., "Mars 2020 Entry, Descent and Landing Instrumentation 2 (MEDLI2)," AIAA Paper 2016-3536, AIAA Thermophysics Conference, June 1016.

[26] Crassidis, J. L. and Junkins, J. L., *Optimal Estimation of Dynamic Systems, Second Edition*, Chapman & Hall, Boca Raton, FL, 2011.

[27] van Loan, C. F., "Computing Integrals Involving the Matrix Exponential," *IEEE Transactions on Automatic Control*, Vol. AC-23, No. 3, 1978, pp. 396–404.

[28] Ektin, B., *Dynamics of Atmospheric Flight*, John Wiley and Sons, Inc., New York, 1972.

[29] Steltzner, A. D., San Martin, A. M., Rivellini, T. P., Chen, A., and Kipp, D., "Mars Science Laboratory Entry, Descent, and Landing System Development Challenges," *Journal of Spacecraft and Rockets*, Vol. 51, No. 4, 2014, pp. 994–1003.

[30] Karlgaard, C. D., Kutty, P., Schoenenberger, M., Munk, M. M., Little, A., Kuhl, C. A., and Shidner, J., "Mars Science Laboratory Entry Atmospheric Data System Trajectory and Atmosphere Reconstruction," *Journal of Spacecraft and Rockets*, Vol. 51, No. 4, 2014, pp. 1029–1047.

[31] Schoenenberger, M., Van Norman, J., Karlgaard, C. D., Kutty, P., and Way, D., "Assessment of the Reconstructed Aerodynamics of the Mars Science Laboratory Entry Vehicle," *Journal of Spacecraft and Rockets*, Vol. 51, No. 4, 2014, pp. 1076–1093.

[32] Bose, D., White, T., Mahzari, M., and Edquist, K., "Reconstruction of Aerothermal Environment and Heatshield Response of Mars Science Laboratory," *Journal of Spacecraft and Rockets*, Vol. 51, No. 4, 2014, pp. 1174–1184.

[33] Karlgaard, C. D., Van Norman, J., Siemers, P., Schoenenberger, M., and Munk, M., "Mars Entry Atmospheric Data System Modeling, Calibration, and Error Analysis," NASA TM-2014-218535, October 2014.

[34] Dyakononv, A., Schoenenberger, M., and Van Norman, J., "Hypersonic and Supersonic Static Aerodynamics Mars Science Laboratory Entry Vehicle," AIAA Paper 2012-2999, June 2012.

[35] Vasavada, A. R., Chen, A., Barnes, J. R., Burkhart, P. D., Cantor, B. A., Dwyer-Cianciolo, A. M., Fergason, R. L., Hinson, D. P., Justh, H. L., Kass, D. M., Lewis, S. R., Mischna, M. A., Murphy, J. R., Rafkin, S. C. R., Tyler, D., and Withers, P. G., "Assessment of Environments for Mars Science Laboratory Entry, Descent, and Surface Operations," *Space Science Reviews*, Vol. 170, 2012, pp. 793–835.

[36] Karlgaard, C. D., Kutty, P., and Schoenenberger, M., "Coupled Inertial Navigation and Flush Air Data Sensing Algorithm for Atmosphere Estimation," *Journal of Spacecraft and Rockets*, Vol. 54, No. 1, 2017, pp. 128–140.

[37] Chen, A., Cianciolo, A., Vasavada, A., Karlgaard, C., Barnes, J., Cantor, B., Hinson, D., Kass, D., Lewis, S., Mischna, M., Rafkin, S., Tyler, D., "Reconstruction of Atmospheric Properties from the Mars Science Laboratory Entry, Descent, and Landing," *Journal of Spacecraft and Rockets*, Vol. 51, No. 4, 2014, pp. 1062–1075.

[38] Way, D., Davis, J., and Shidner, J., "Assessment of the Mars Science Laboratory Entry, Descent, and Landing Simulation," AAS Paper 13-420, February 2013.